www.sciencemag.org/cgi/content/full/1144124/DC1

Supporting Online Material for

Toward Direct Measurement of Atmospheric Nucleation

Markku Kulmala,* Ilona Riipinen, Mikko Sipilä, Hanna E. Manninen, Tuukka Petäjä, Heikki Junninen, Miikka Dal Maso, Genrik Mordas, Aadu Mirme, Marko Vana, Anne Hirsikko, Lauri Laakso, Roy M. Harrison, Ian Hanson, Carl Leung, Kari E. J. Lehtinen, Veli-Matti Kerminen

*To whom correspondence should be addressed. E-mail: markku.kulmala@helsinki.fi

Published 30 August 2007 on *Science* Express

DOI: 10.1126/science.1144124

This PDF file includes:

Supporting online material

for the manuscript entitled 'Towards direct measurement of atmospheric nucleation' by Kulmala *et al.*

Materials and methods

Balanced Scanning Mobility Analyzer (BSMA)

The BSMA (*S1*) is an instrument capable of measuring mobility distributions of small air ions and naturally charged nanoparticles (intermediate ions) of both negative and positive polarity. The mobility range of the BSMA is 3.2 to 0.032 $cm^2\ V^{-1}\ s^{-1}$, which corresponds to a mobility diameter range of 0.8 to 7.6 nm. The BSMA consists of two plain aspiration condensers, one for each polarity, and a common electrical amplifier connected to a balanced bridge circuit. The BSMA has been designed in the University of Tartu and built by Airel Ltd.

Size segregation is obtained by varying the electric field via a discharge of a capacitor through the repelling electrode and monitoring the electrometer current in the balanced bridge circuit. During the relaxation time (19 seconds), ion mobility distributions covering two orders of magnitude are monitored. An inlet gate lets either positive or negative ions pass through the aspiration condenser. During the electrometer offset measurements all the ions are filtered away with the inlet gate. In a normal measurement cycle the BSMA measures the mobility distributions of negative and positive ions, and the offset in an alternating manner (*S1*). The data is averaged over 10 minutes. A more detailed description of the instrument can be found in a paper by Tammet (2006) (*S1*) and examples of its atmospheric applications in a study by Hirsikko et al. (2006) (*S2*).

Air Ion Spectrometer (AIS)

The AIS (*S3*) (Airel Ltd., Estonia) measures mobility distributions of both negative and positive air ions in the range from 3.16 to 0.00133 $cm^2\ V^{-1}\ s^{-1}$. This corresponds to a diameter range of approximately 0.8 to 40 nm. In essence, the AIS consists of two cylindrical Differential Mobility Analyzers (DMAs) equipped with insulated

electrometer rings. Sampled ions are collected on the electrometer rings in 21 electrical mobility fractions simultaneously for both polarities.

Neutral Cluster - Air Ion Spectrometer (NAIS)

The NAIS is an instrument which measures sub-3 nm neutral and charged aerosol particles and clusters. The measurement principle of the NAIS is based on unipolar charging of sampled particles and their subsequent detection with an electrical mobility analyzer.

The NAIS is developed from the Air Ion Spectrometer (AIS, Airel Ltd., Estonia). It has 21 electrometer rings in the inside-out differential mobility analyzers. Unlike the AIS, the NAIS has two unipolar corona chargers prior to the mobility analyzers - one for positive and one for negative charging - and electrostatic post filters. These post filters are used to remove the ions generated by the chargers. The particle charging probabilities are estimated from Fuchs' theory (*S4*) and discussed in the next section. The lower detection limit of the NAIS is determined by the charging probabilities, cluster concentration and the charger ion masses and mobilities. The charger ion mobilities from 1.3 to 1.6 $cm^2 V^{-1} s^{-1}$ define the lowest estimation for the detection limit, which is approximately 1 nm. Particles below this limit cannot reliably be distinguished from the charger ions.

The sample and sheath flows of the analyzers are 0.5 $l s^{-1}$ and 1 $l s^{-1}$, respectively. A closed loop sheath flow arrangement is used in both analyzers. The noise and the offset of the electrometers are measured by sampling through a second filter consisting of a unipolar corona charger and an electrostatic filter. Similar filtration is used also for cleaning the re-circulated sheath air.

As an example, a two hour mean aerosol number distributions from Hyytiälä on April 24, 2006 are presented in Fig. S1. Figure S1a shows size distributions measured during new particle formation at 12:00–14:00. The corresponding two hour mean distributions for the night time (00:00–02:00) are presented in Figure S1b. The NAIS is in qualitative agreement with a conventional Differential Mobility Particle Sizer (DMPS) (*S5*) in the overlapping size range. Below the DMPS detection limit (d_p = 3

nm), the NAIS detects a large number of clusters, which form a clear separate mode to sizes larger than the ions produced by the corona charger. The charger ions, on the other hand, can be seen in Fig. S1 at the smallest sizes of the distribution measured in the negative mode of the NAIS. The differences between the polarities in the lowest channels of NAIS are due to the operation of the post-filter. The positive post-filter successfully removes all the charger ions, but the negative post-filter lets a fraction of the cluster ions generated inside the charger to pass into the lowest electrometer channels.

The concentration of particles based on two electrometer currents (channels 5 and 6) of the NAIS instrument during two consecutive days (April 23–24, 2006) are depicted in Fig. S2. The channels correspond to particles 1.8–2.4 nm and 2.4–3.0 nm in mobility diameter (Millikan-Fuchs equivalent diameter). The concentrations in the negative and positive sides of the NAIS follow each other during April 23. Both of the channels show a clear maximum around noon and a minimum during the night. The channel 5 readings suggests that there is always a background concentration of the order of 500–1000 cm^{-3} in the size range of 1.8–2.4 nm. In channel 6 (2.4–3.0 nm) the concentration approaches zero during the night time. The agreement between the polarities, however, deteriorates during the following day. Based on the ion-DMPS (*S6*), on April 23 the charging state of the formed nanoparticles was close to steady state charge distribution, whereas on the following day, the charged fraction of the freshly nucleated particles exceeded that of the steady state.

Particle charging probability in the NAIS

The aerosol charging follows the theory originally presented by Fuchs and Sutugin (*S4*), and the charging inside the limiting sphere is calculated using the kinetic theory (*S7*). The charging efficiency is described via charging parameter $\alpha = \frac{1}{\varepsilon_0}\int \lambda dt$, where $\lambda = ekn$ is the air electrical conductivity (*S8*), e is the elementary charge, k is the ion electric mobility, and n is the ion concentration in the charger volume.

The charging probabilities using a calibrated charging parameter $\alpha = 6$, which translates to $nt = 2.22 \times 10^6$ for mobility 1.5 $cm^2/V/s$, are presented in Table S1 and Fig. S3. Particle initial charge is 0 *e*.

Condensation Particle Counter UF-02proto

The UF-02proto CPC is a swirling flow type CPC described in detail by Mordas et al. (2005) (*S9*). The instrument uses butanol as the condensing vapour and at normal operation settings its 50%-detection limit (cut-off size, D50) is ca. 4.3 nm (*S9*). In this work the CPC has been used in the conductive cooling mode.

We improved the detection limit of UF-02proto by adjusting the temperature difference between the saturator and the condenser. The cut-off size was determined using silver aerosol generated in a tube furnace. A fraction of the aerosol was extracted in a differential mobility analyzer (DMA, HAUKE 109 mm). The DMA was operated with a sheath flow of ca. 22 l min^{-1} and an aerosol flow of 2-3.5 l min^{-1}. An electrometer (TSI-3068) was used as a reference.

Increasing the temperature difference between the saturator and the condenser improved the detection limit significantly. A calibration curve with a temperature difference of 44 ºC is presented in Figure S4. The D50, is 1.8±0.3 nm. It can be considered very competent in the field of conductive cooling type CPCs. Since the DMA transfer functions are relatively wide at sub-3 nm particle sizes (*S10*), a correction that takes into account the estimated original size distribution was applied.

A further increase of the temperature difference did not affect the detection limit any more (Fig. S5), but increased the concentration of homogeneously nucleated particles inside the CPC. The effect of the background aerosol population on the detection limit was investigated at a temperature difference of 48 ºC. Calibrations with a background concentration of 3000 cm^{-3} yielded the same detection limit within the error estimations.

Three separate UF-02proto CPCs were used in the field campaign. The cut-off diameters of the instruments were tuned to 1.8, 2.5 and 3 nm. The detection efficiency

curves as a function of particle size were verified in the laboratory. Due to a minor drift of the CPC flows during the field measurements, the concentrations measured by the CPCs were normalized to match during night-time. Thus we were only able to follow the concentration changes in the size range between 1.8 and 3 nm based on the different UF-02proto CPCs. The trend of the sub-3 nm concentration measured with the CPCs, however, agreed with the trend measured by the NAIS.

Electrical Mobility Spectrometer

The electrical mobility spectrometer (EMS) used at the University of Birmingham consisted of a Grimm (Grimm Aerosol Technik, Ainring, Germany) Vienna type nano-DMA in combination with a highly sensitive GRIMM Faraday Cup Electrometer (FCE). Atmospheric particles were ionised using a recently developed unipolar corona ioniser (*S11*).

The Grimm FCE is a highly sensitive (up to 0.1 fA at 1 Hz) electrometer that allows direct counting of charged airborne particles. Using a FCE has many advantages over the more traditional Condensation Particle Counters (CPCs) in that no magnification of particles is necessary, thus removing the need of both condensation agents and temperature control whilst at the same time optical and laser parts are also not needed. In this instrument the aerosol sample is drawn through a Faraday Cup Filter which is isolated and connected to a highly sensitive electrometer and amplifier. The amount of electrical charge passing through the filter at a certain time is measured as an electrical current which, along with the sample airflow and charging efficiency, can be used to calculate particle concentrations. This FCE is able to measure charged airborne particles in the size range of 0.8 nm to 700 nm and is especially adapted to measure very small particles up to very high concentrations.

Separation of atmospheric particles prior to counting in the FCE is carried out by a GRIMM Vienna type nano-DMA (*S12*). In this design the sample aerosol enters the DMA through a tangential inlet and is introduced to the particle-free sheath flow in the electrostatic column via a narrow annular slit. A potential is applied across the inner and outer electrode of the electrostatic column using an external high-precision HV supply. The charged particles then migrate across this region according to their electrical

mobilities (as given by particle diameter). By varying the applied voltage the diameter of particles leaving the exit aperture can be controlled. To minimise particle losses the DMA sample outlet is connected directly to the sample inlet of the FCE.

The airflows (sample and sheath) and voltages are controlled by a DMA controller and can be adjusted via software installed on a connected PC. The controller manages all the voltage settings of the DMA, the electrical adjustments of the FCE and acquires and monitors all the data from the DMA, FCE and ancillary sensors. All experiments were conducted at sample flow rates of 5 l min^{-1} and at sheath flows of 20 l min^{-1} which corresponds to aerosol sizes of 0.8–38 nm in diameter.

Charging of atmospheric particles is achieved using a unipolar corona ioniser. The design of the ioniser is very simple and consists, in brief, of a stainless steel electrode ended in a sharp tip and held coaxially to a grounded external cylinder. A high voltage is applied to the tip via an external HV supply which results in a high electrostatic field at the electrode point. It has been shown (*S12, S13*) that charging efficiencies as high as 30% can be achieved for 10 nm particles. The ioniser was connected to both external atmosphere and the DMA inlet using as short a tubing as possible (to minimise diffusion losses) and was operated in the negative ion mode. Switching off the corona charger allowed the signal due to air ions to be determined and this did not generally rise above the noise level of the detector, demonstrating that the particles observed are neutral clusters.

Particle formation measured using several different instruments

To illustrate typical new particle formation observed simultaneously with the instrumentation described above, surface plots of the particle size distributions observed with the DMPS, BSMA, AIS and NAIS on April 23, 2006 and April 24, 2006 are presented in Figures S6 – S9. The measurements have been conducted at the SMEAR II station in Hyytiälä, southern Finland. The station is located at a rural site, surrounded by pine-dominated forests. The station is equipped with extensive instrumentation for atmospheric measurements (*S14*). Clear new particle formation starting before noon and the subsequent growth of the particles is observed with all the instruments.

We also demonstrate the presence of neutral clusters in Birmingham, England using an electrical mobility spectrometer currently able to measure particles from 1.8 to 38 nm diameter. The data, collected in the months of May and July 2006 are currently in the form of detector current which shows a strong diurnal cycle in particles of 1.8-3 nm in diameter, with number concentrations increasing after sunrise, peaking in the early afternoon and decreasing slowly through the evening, typically falling near zero around midnight (see Fig. S10). Our earlier work at this site has shown that bursts of new particles (> 3 nm diameter) are produced relatively infrequently (8–12 days out of 232) (S*15*) with no formation observed during the May/July 2006 sampling campaign.

Determination of J_2 from the observed size distribution evolution

The time evolution of the number concentration of 2–3 nm particles ($N_{2\text{-}3}$) is described by the balance equation

$$\frac{\mathrm{d}N_{2-3}}{\mathrm{d}t} = GR_2 \cdot n_2 - GR_3 \cdot n_3 - CoagS_{2-3} \cdot N_{2-3}, \qquad \text{(S1)}$$

including terms for the growth into the 2–3 nm range over the 2 nm limit (in practice 1.8 nm), out of the range over the 3 nm limit, and the loss by coagulation scavenging. The function n is the particle size distribution function, defined as $n = \mathrm{d}N/\mathrm{d}d_p$. $CoagS_{2\text{-}3}$ denotes the average coagulation sink for the 2–3 nm range (*S16*). By rearranging the terms, and denoting the first term on the right hand side of Eq. S1 by J_2, the following equation is obtained:

$$J_2 = \frac{\mathrm{d}N_{2-3}}{\mathrm{d}t} + CoagS_{2-3} \cdot N_{2-3} + \frac{f}{1.2\,\mathrm{nm}} GR_3\, N_{2-3} \ . \qquad \text{(S2)}$$

J_2 is the apparent nucleation rate, i.e. the formation rate of new particles into the measurable range of above 2 (in practice 1.8) nm. Here the coagulation loss (second term on the right hand side) for the interval 1.8–3 nm has been approximated by a term representing the loss of 2 nm sized particles, directly calculated from the measured

background particle size distribution, with hygroscopicity effects estimated as by Laakso et al. (*S17*). The third term representing the condensation loss out of the size range 1.8–3 nm results from approximating n_3 by $N_{2\text{-}3}$/(3nm – 1.8nm). The left hand side of Eq. S1, the change in the 1.8–3 nm particle number concentration, is directly obtained from the NAIS or CPC measurements. The factor f represents the fraction of the 2-3 nm particles which are activated for growth. In this work we assumed f = 1, thereby calculating the upper limits for the formation rates.

In the case of charged particles, the ion-ion recombination and the charging of 2–3 nm neutral particles need to be taken into account. The formation rate of 2–3 nm charged particles can therefore be expressed as

$$J_2^{\pm} = \frac{\mathrm{d}N_{2-3}^{\pm}}{\mathrm{d}t} + CoagS_{2-3} \cdot N_{2-3}^{\pm} + \frac{1}{1.2\,\mathrm{nm}} GR_3\, N_{2-3}^{\pm} + \alpha \cdot N_{2-3}^{\pm} N_{<3}^{\mp} - \beta \cdot N_{2-3} N_{<3}^{\pm}, \qquad \text{(S3)}$$

where $N^{\pm}_{2\text{-}3}$ refers to the 2–3 nm charged particle concentration, and $N^{\pm}_{<3}$ is the ion concentration below 3 nm. α is the ion-ion recombination coefficient and β refers to the ion-neutral attachment coefficient. The ion concentrations were obtained from the AIS data, the coagulation sink from the DMPS data, and the particle growth rates were determined from the BSMA data. The values α and β were $1.6 \cdot 10^{-6}$ $\mathrm{cm^3 s^{-1}}$ and $0.01 \cdot 10^{-6}$ $\mathrm{cm^3 s^{-1}}$, respectively (*S13*).

The particle concentrations used in Eqs. S2 and S3 were approximated with the median concentrations during the new particle formation event. The formation rates J_2 for the total aerosol concentrations (determined from the both polarities of NAIS and the UF-02proto CPCs) and for the ions (determined from both polarities of AIS) are presented for four exemplary days (April 23, April 24, April 30, and May 10) in Table S2. April 24 and May 10 were days with significant overcharging, whereas on April 23 and 30 the aerosol was undercharged or very close to the steady state charge distribution.

Balance equations for neutral and charged cluster concentrations

The number concentrations of neutral and charged cluster can be estimated by solving simple balance equations. As a bonus, we get estimations on the relative roles of neutral and ion induced nucleation on observed particle formation events.

The rate at which clusters are activating can be written as

$$\frac{dN_{act}}{dt} = IN_{clus} \ , \tag{S4}$$

where N_{act} is the number concentration of activated clusters, or aerosol particles, N_{clus} is the cluster number concentration, and I is the heterogeneous nucleation rate per one cluster. Since the activation takes place close to the 2 nm in diameter, we may further write

$$\frac{dN_{act}}{dt} \cong J_2 \ . \tag{S5}$$

Here J_2 is formation rate of 2 nm particles obtained from measurements (NAIS, CPCs, BSMA and AIS), and is given by

$$J_2 = J_{2,n} + J_{2,i} , \tag{S6}$$

where $J_{2,n}$ and $J_{2,i}$ refer to the activation of neutral clusters and ions, respectively. By combining Eqs. S4–S6 we finally obtain:

$$J_2 = I_i N_i^{\pm} + I_n N_n \ . \tag{S7}$$

Here $N_i^{\pm}$ is number concentration of ion clusters of sign ± and N_n is the number concentration of neutral clusters that have not yet been activated. These neutral clusters may originate from homogeneous nucleation, ion-ion recombination or some chemical reactions.

Next, let us make an order of magnitude estimate on the minimum number concentration of neutral clusters, $N_{n,min}$, and the maximum concentration of neutral clusters due to ion-ion recombination, $N_{n,rec,max}$. According to our measurements, $N_i^{\pm} \approx$ 1000 cm^{-3} and J_2 and $J_{2,i}$ were about 1 and 0.1 cm^{-3} s^{-1}, respectively. For thermodynamic reasons, $I_n \leq I_i$. The value of $N_{n,min}$ is obtained by setting $I_n = I_i$, which leads to $N_{n,min} \approx 10^4$ cm^{-3}.

The set of balance equations describing the time evolution of the neutral cluster concentration due to ion-ion recombination alone may be written as:

$$\frac{dN_{n,rec}}{dt} = a\alpha N_i^+ N_i^- - 2\beta N_{n,rec} N_i^{\pm} - \mathrm{CoagS}(N_{n,rec}) \cdot N_{n,rec}\,, \qquad \text{(S8)}$$

where a is the probability that a collision between two ions of opposite sign lead to the formation of a stable neutral cluster. At steady state,

$$N_{n,rec} = \frac{a\alpha N_i^+ N_i^-}{\mathrm{CoagS}(N_{n,rec}) + 2\beta N_i^{\pm}}\,. \qquad \text{(S9)}$$

The value of the coagulation sink depends on the nuclei size and pre-existing particle number size distribution, and it is expected to be somewhat larger for the ion clusters than for neutral clusters. In most cases, the second term in the denumerator of equation (S9) is small compared with the first term in it, so we may write

$$N_{n,rec} = \frac{a\alpha N_i^{\pm}}{CoagS(N_{n,rec})} \qquad \text{(S10)}$$

The minimum value of CoagS in Hyytiälä is about 10^{-4} s^{-1}, which gives $N_{n,rec,max} \approx 10^4$ cm^{-3} when assuming $a = 1$. As $N_{n,rec,max} \approx N_{n,min}$, we may conclude that in the extreme case with conditions most favourable for the ion-ion recombination, this process could explain almost totally the pool of unactivated neural clusters.

However, we studied several days with measured values of J_2 in more detail. We calculated the coefficients I, the lower-limit predictions for the values of N_n based on Eqs S4 – S7, as well as approximations for the number of neutral clusters produced by ion-ion recombination $N_{n,rec}$. We calculated $N_{n,rec}$ first by assuming a = 1 (i.e. all the formed clusters are stable, to get an estimate for the upper limit), and then assuming that only clusters larger than 1000 amu stay stable. The results are presented in Table S3.

As a main result, on only one of the four investigated days (10.5. 2006), the maximum contribution of recombination to N_n reaches 10 %. During that day the ions and their recombination is able to explain about 30% of the particle formation. In all other days this contribution is much less than 10%. Also if we use the physically more probable value of a=a(1000amu), we see that the contribution of recombination is almost negligible.

Theoretical calculation of cluster concentrations in the size range 1.8-3.0 nm

The total concentration of clusters in the size range 1.8 – 3.0 nm, N_{tot}, can be calculated from the following formula (*S18*):

$$N_{tot} = \frac{J_3}{GR}\exp(-\eta / d_1)\times \left[d_1 \exp(\eta / d_1) - d_0 \exp(\eta / d_0) + \eta \ln(d_1 / d_0) + \sum_{k=1}^{\infty} \frac{\eta^{k+1}(d_0^{-k} - d_1^{-k})}{k \cdot k!} \right] \quad \text{(S11)}$$

Here d_0 = 1.8 nm, d_1 = 3.0 nm, J_3 is the formation rate of 3 nm particles, GR is the average cluster growth rate in the size range 1.8-3 nm and the parameter η is given by $\eta \approx 0.23 \cdot CS'/GR$, where CS' is the condensation sink. In order to apply Eq. S11, we need to know J_3, CS' and GR. The first two of these quantities are obtained from the DMPS measurements, and GR is estimated based on the BSMA data.

In a strict sense, Eq. S11 is valid only when there is a roughly constant flux of growing clusters across the 3 nm diameter limit. Thus, any sudden changes in J_3 lead to values of N_{tot} that deviate from the real concentration of clusters in the size range 1.8–3.0 nm. Equation S11 is extremely sensitive to the cluster growth rate, GR. Since this quantity is difficult to determine accurately, there is an inherent uncertainty in the calculated value of N_{tot} that cannot be avoided. It should finally be noted that Eq. S11 counts only the "dynamically active" clusters, that is, clusters that are growing in size toward 3 nm. As a result, if only a portion of the clusters in the size range 1.8–3.0 nm have been activated for growth, N_{tot} given by Eq. S11 seriously under-predicts the real concentration of 1.8–3.0 nm clusters.

Supporting figures

a)

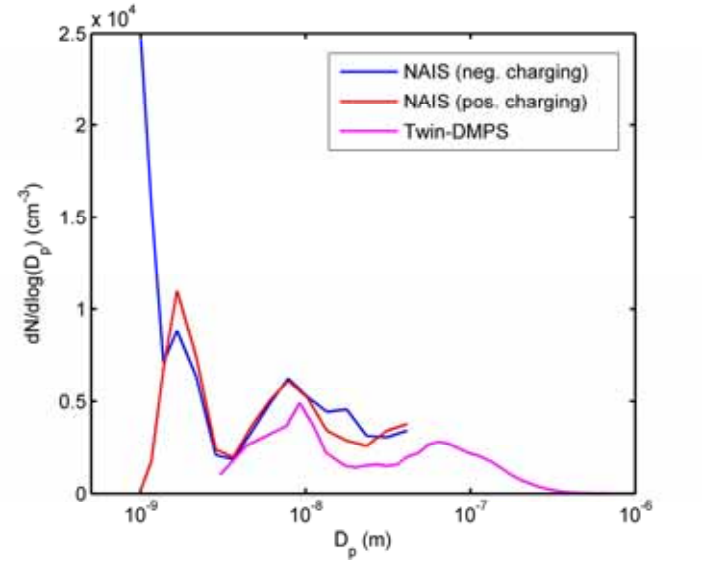

b)

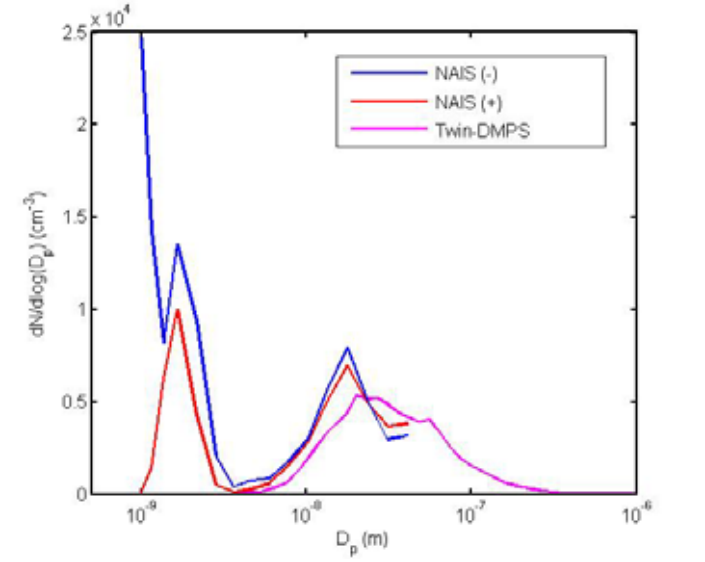

Figure S1. Two-hour average number size distributions measured with NAIS and DMPS during a new particle formation event on April 24, 2006; a) during new particle formation at 12:00–14:00; b) at 00:00–02:00, when no new particle formation is observed.

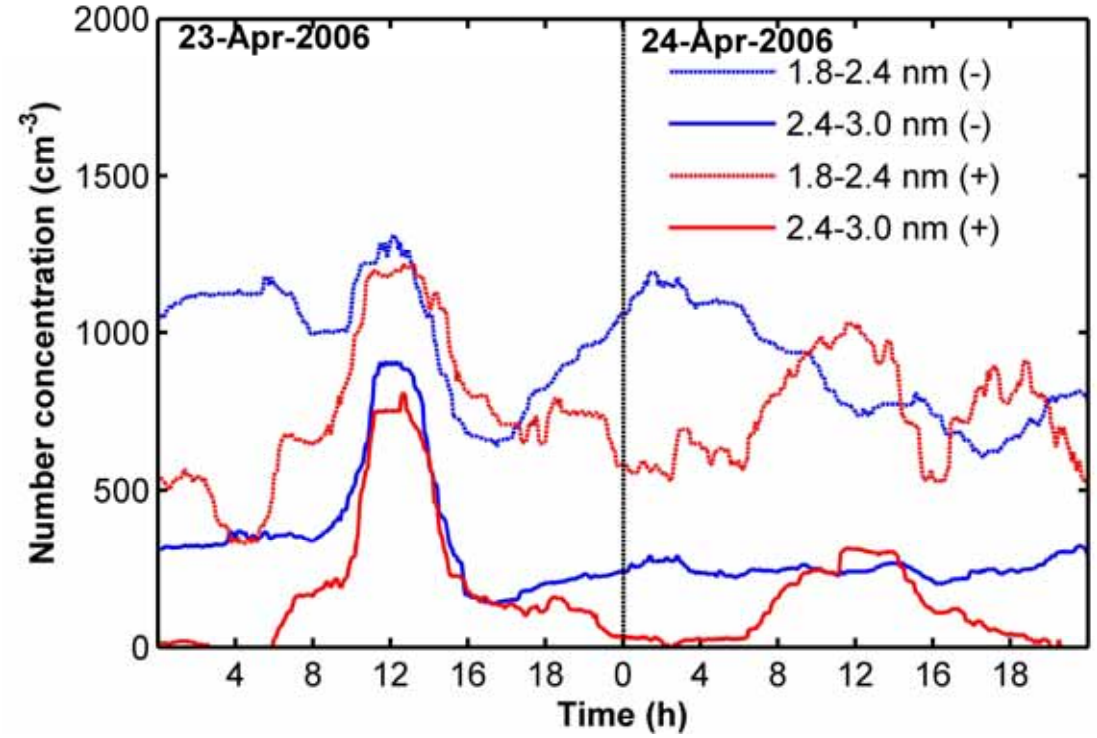

Figure S2. Aerosol particle number concentrations measured with two NAIS electrometers corresponding to the size ranges 1.8–2.4 nm (channel 5) and 2.4–3.0 nm (channel 6) on April 23, 2006, and April 24, 2006.

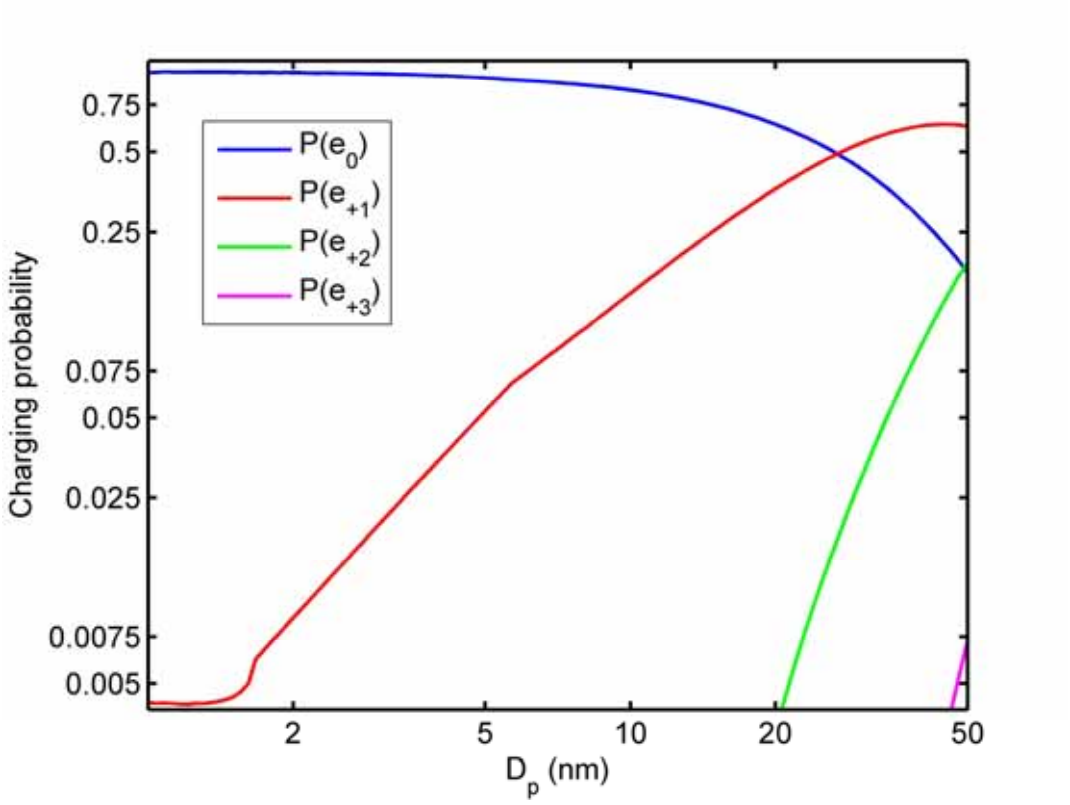

Figure S3. The NAIS Charging probability. Charged fraction as a function of size. Note the fraction of double charged particles at large particle sizes in the unipolar charger.

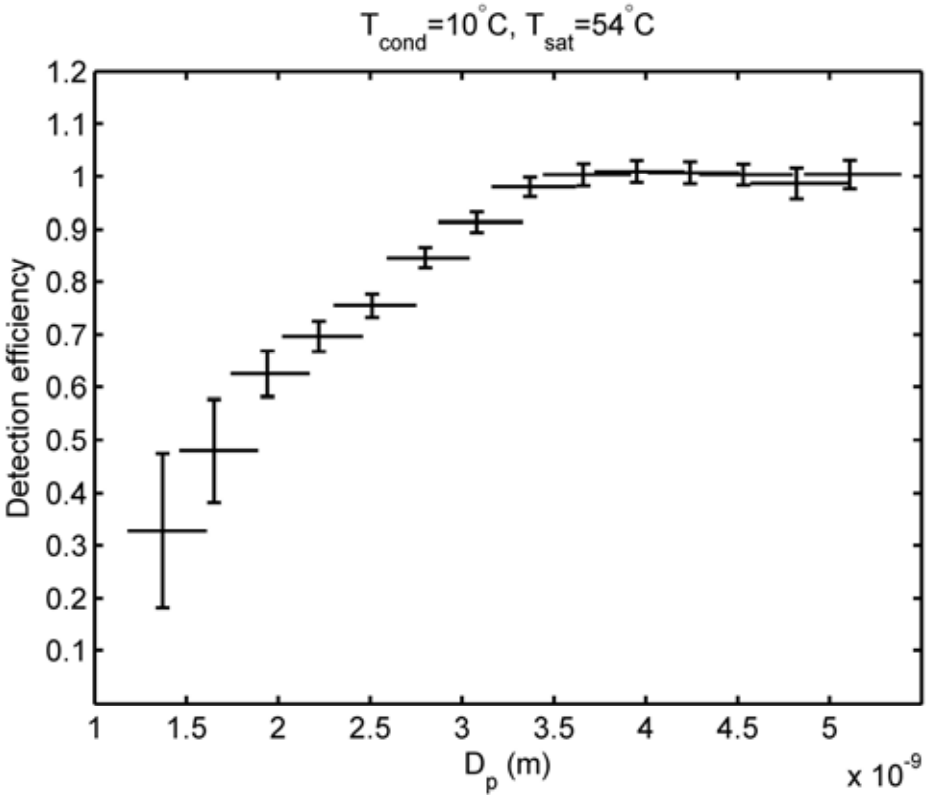

Figure S4. The detection efficiency of the UF-02proto CPC with a temperature difference of 44 ºC between the saturator and the condenser.

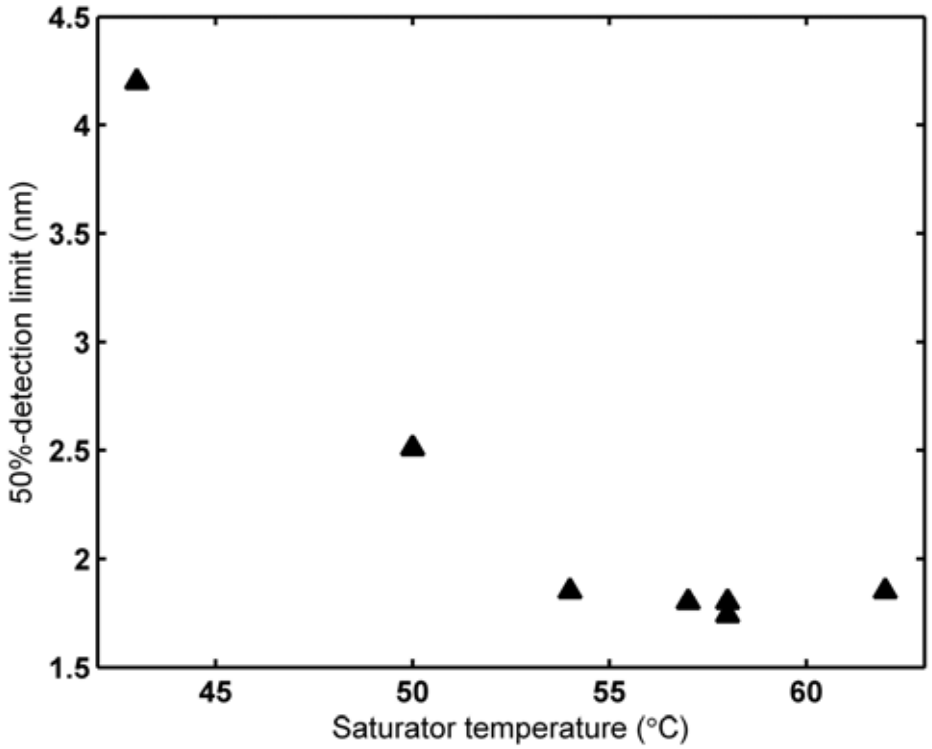

Figure S5. The cut-off size of the UF-02proto CPC with different saturator temperatures, while the condenser temperature is kept constant at 10 ºC. The saturator temperature of 43 ºC corresponds to the normal operation settings.

a)

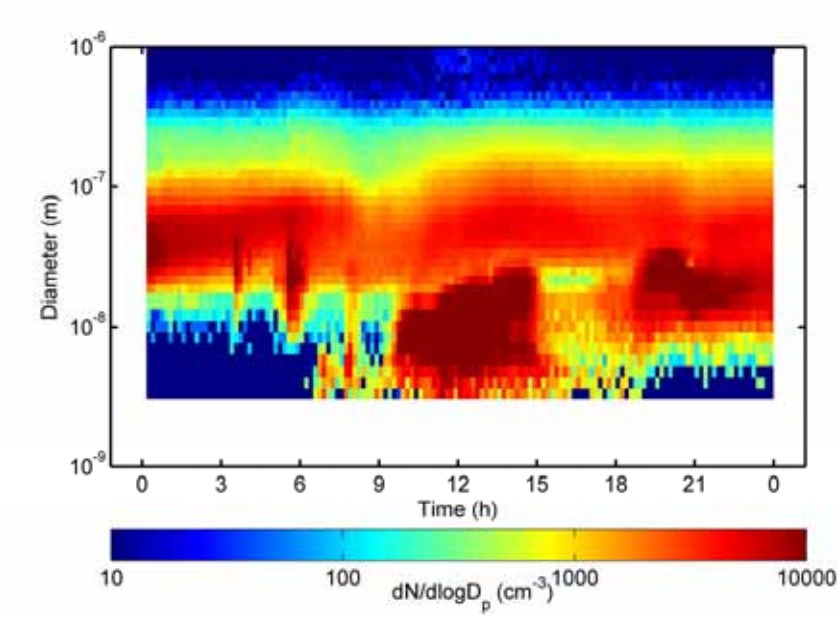

b)

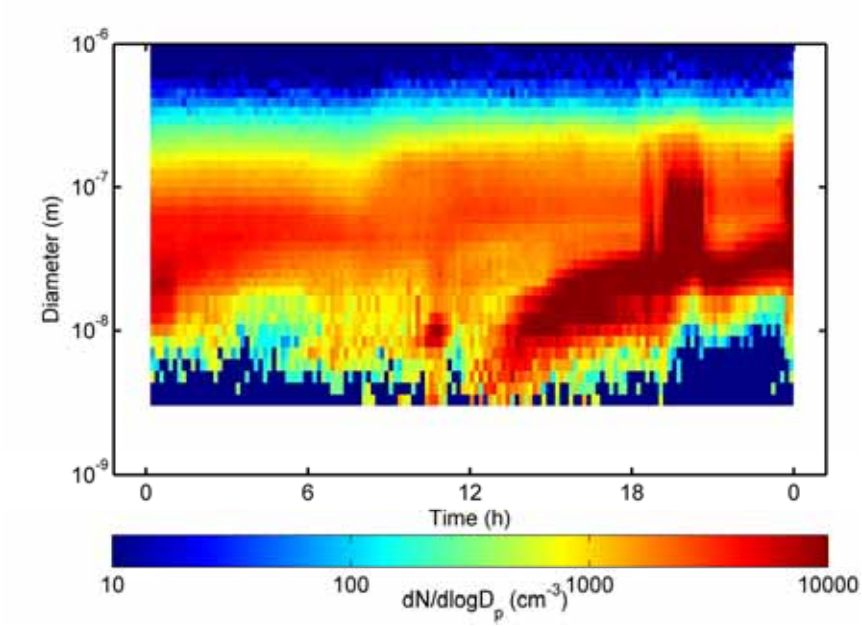

Figure S6. A surface plot of the particle number size distributions measured using the DMPS on two particle formation event days (a: April 23, 2006, b: April 24, 2006).

a)

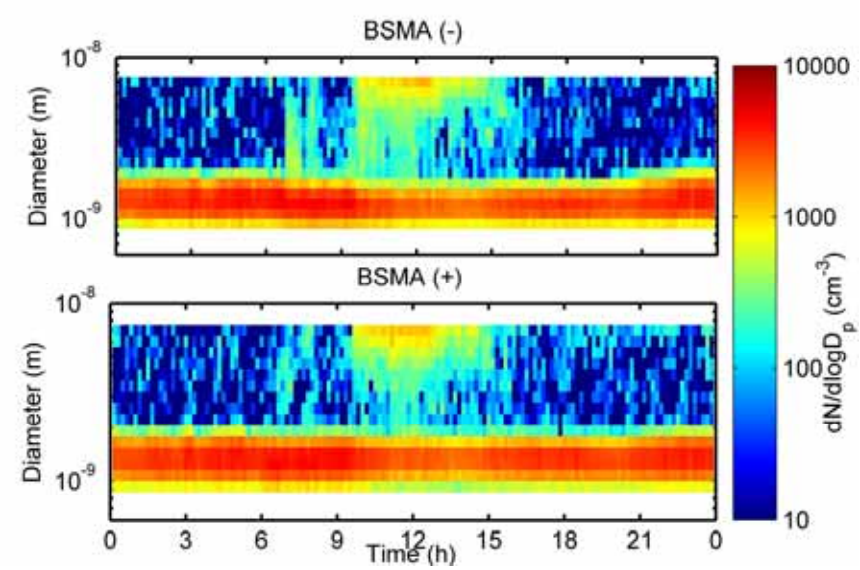

b)

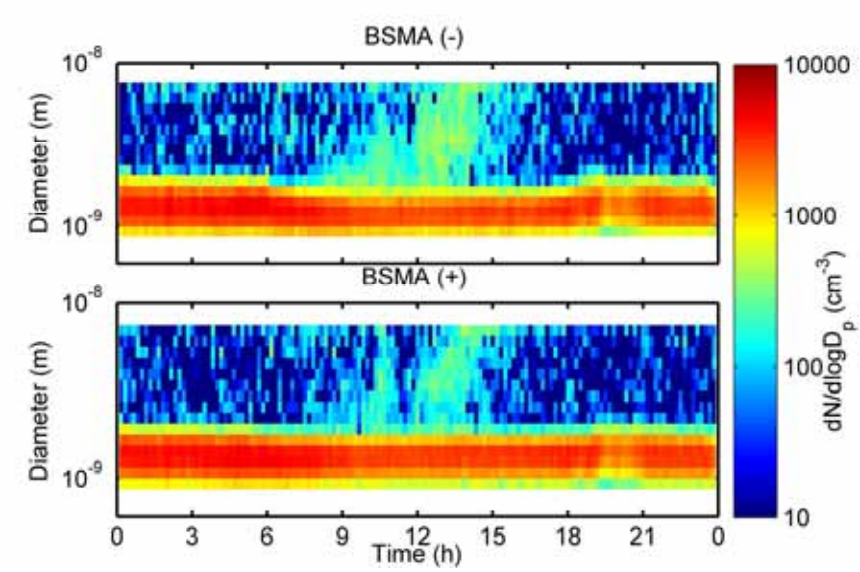

Figure S7. A surface plot of the particle number size distributions measured using the BSMA on two particle formation event days (a: April 23, 2006, b: April 24, 2006).

a)

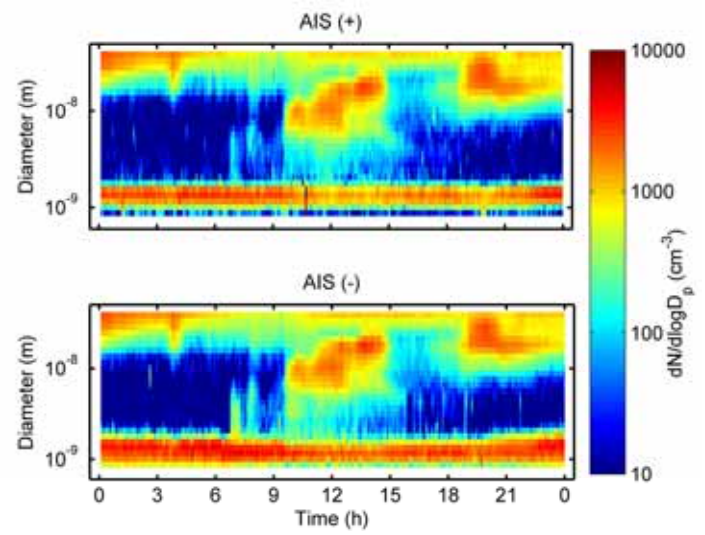

b)

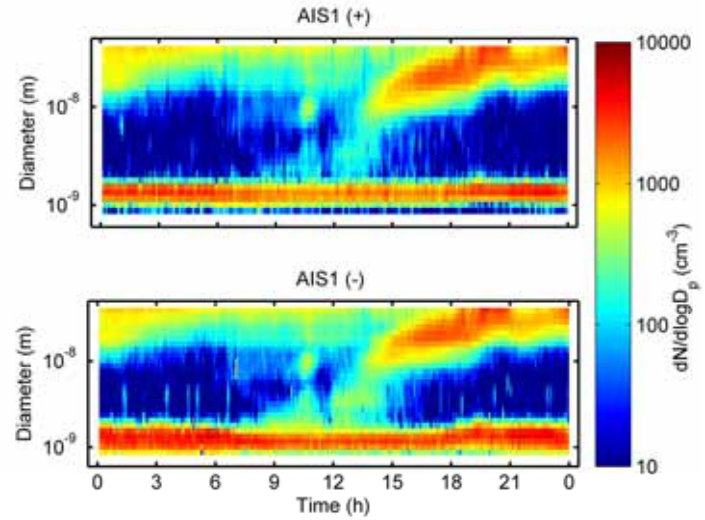

Figure S8. A surface plot of the particle number size distributions measured using the AIS on two particle formation event days (a: April 23, 2006, b: April 24, 2006).

a)

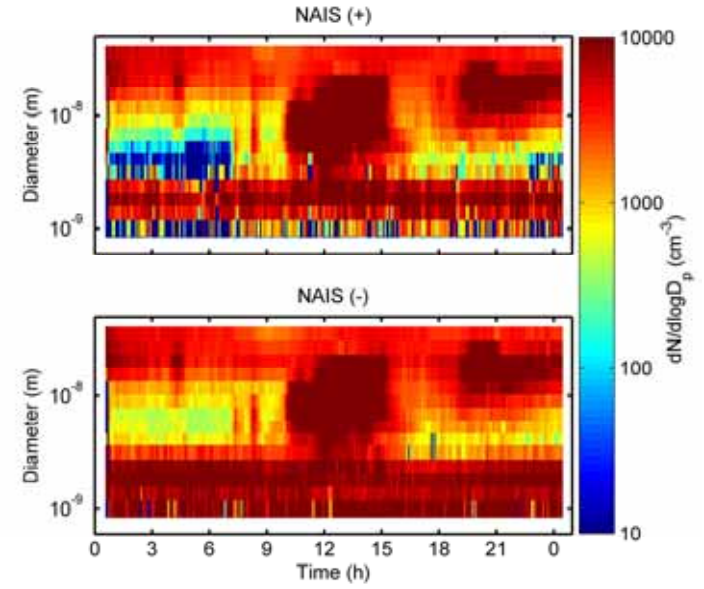

b)

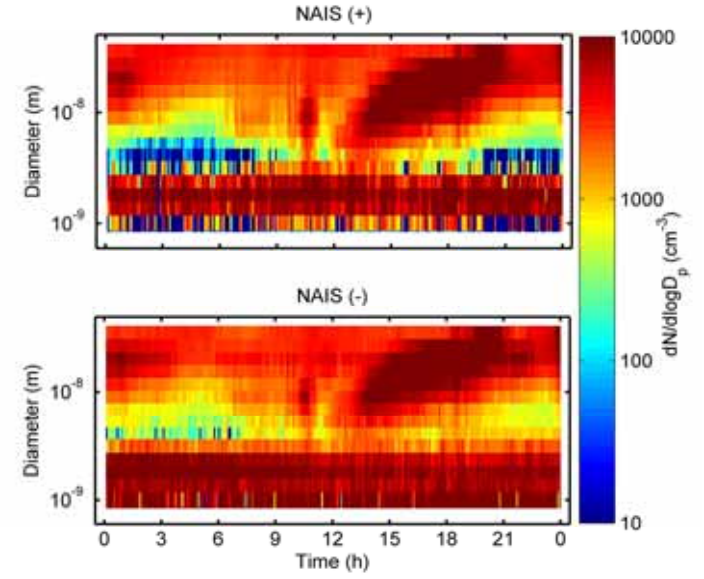

Figure S9. A surface plot of the particle number size distributions measured using the NAIS on two particle formation event days (a: April 23, 2006 b: April 24, 2006).

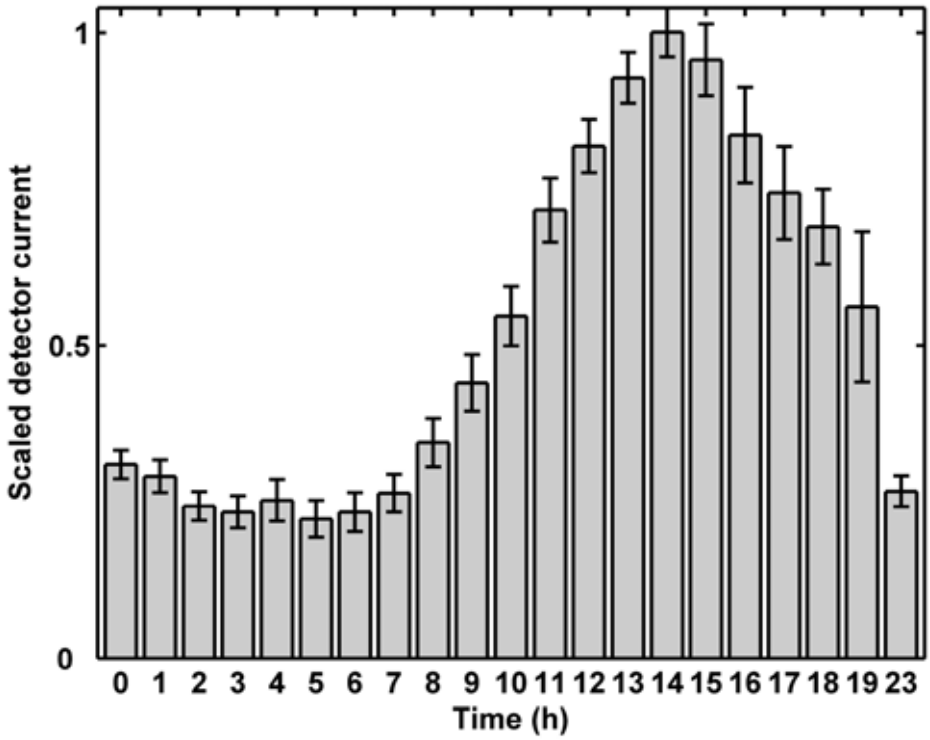

Figure S10. The diurnal variation of the EMS detector current which indicates the concentration of 1.8–3.0 nm clusters in Birmingham, UK 22.08.2006 – 29.08.2006. The bars are the arithmetic mean of raw 5 min data scaled with the maximum value. The whiskers indicate the standard error of the mean.

Supporting tables

Table S1. Parameters (mean charge, the standard deviation of the charge distribution, the charging probabilities) of the charge distribution (elementary charges) of the NAIS as a function of the particle size.

D_p(nm)	Mean Q	STD Q	$P(e_0)$	$P(e_{+1})$	P (e_{+2})	P (e_{+3})
1.28	0.0043	0.065	0.997	0.0043	0.0000	0.0000
1.47	0.0044	0.066	0.995	0.0044	0.0000	0.0000
1.70	0.0049	0.07	0.994	0.0049	0.0000	0.0000
1.97	0.0072	0.084	0.993	0.0072	0.0000	0.0000
2.27	0.0095	0.097	0.989	0.0095	0.0000	0.0000
2.62	0.013	0.11	0.987	0.0126	0.0000	0.0000
3.03	0.017	0.13	0.983	0.0168	0.0000	0.0000
3.50	0.022	0.15	0.978	0.0224	0.0000	0.0000
4.04	0.03	0.17	0.971	0.0296	0.0000	0.0000
4.66	0.049	0.22	0.950	0.0493	0.0000	0.0000
5.38	0.059	0.24	0.941	0.0593	0.0000	0.0000
6.22	0.072	0.26	0.929	0.0718	0.0000	0.0000
7.18	0.088	0.28	0.913	0.0876	0.0000	0.0000
8.29	0.11	0.31	0.892	0.1076	0.0000	0.0000
9.58	0.13	0.34	0.868	0.1316	0.0000	0.0000
11.06	0.16	0.37	0.839	0.1615	0.0000	0.0000
12.77	0.2	0.4	0.803	0.1973	0.0000	0.0000
14.75	0.24	0.43	0.759	0.2410	0.0000	0.0000

17.03	0.29	0.46	0.708	0.2908	0.0006	0.0000
19.66	0.35	0.48	0.650	0.3476	0.0025	0.0000
22.70	0.42	0.51	0.584	0.4089	0.0065	0.0000
26.22	0.5	0.53	0.512	0.4733	0.0142	0.0000
30.28	0.59	0.55	0.436	0.5358	0.0284	0.0001
34.96	0.7	0.57	0.358	0.5895	0.0529	0.0003
40.38	0.81	0.59	0.281	0.6245	0.0923	0.0012
46.62	0.95	0.61	0.212	0.6339	0.1515	0.0039
53.84	1.1	0.65	0.149	0.6088	0.2297	0.0115

Table S2. The calculated 2 nm formation rates for total aerosol particle concentrations (both polarities of NAIS and UF-02proto CPC) and charged particles (both polarities of AIS) on four exemplary days with new particle formation. On days 24.4. and 10.5. clear overcharging was observed for both polarities. On 30.4. the ambient aerosol was clearly undercharged. On 10.5. the growth rates $GR_{1\text{-}3}$ were available for both BSMA polarities, therefore giving two values for the J_2. On the rest of the days the $GR_{1\text{-}3}$ estimates were available only for the negative BSMA data.

Date	J_2 (NAIS+) (cm^{-3} s^{-1})	J_2 (NAIS-) (cm^{-3} s^{-1})	J_2 (UF-02proto) (cm^{-3} s^{-1})	J_2 (AIS+) (cm^{-3} s^{-1})	J_2 (AIS-) (cm^{-3} s^{-1})
23.4.2006	1.5	1.6	1.1	0.04	0.02
24.4.2006	1.7	-	1.3	0.04	0.07
30.4.2006	2.8	2.2	-	0.03	0.06
10.5.2006	0.8/1.2	0.5/1.1	-	0.07/0.08	0.06/0.09

Table S3. The total and charged particle formation rates at 2 nm, activation coefficients and the numbers of neutral clusters during four new particle formation events in spring 2006. The estimated concentrations of neutral clusters due to recombination are also presented. The larger value corresponds to the case when all recombination products are stable, and the smaller one to the cases when only recombination products larger than 1000 amu are assumed to be stable. To obtain a maximum estimate for the recombination products, we have used the smallest values of J_2 obtained for each day. The estimations have been made using the positive ion formation rates.

Date	J_2 / $J_{2,I}$ (cm^{-3} s^{-1})	I_i (s^{-1})	N_n (cm^{-3})	$N_{n,rec}$ (a = 1) / $N_{n,rec}$ (a = a(1000amu)) (cm^{-3})
23.4.2006	1.1 / 0.04	5.9e–5	18500	833 / 156
24.4.2006	1.3 / 0.04	1.67e-4	7800	175 / 95
30.4.2006	2.2 / 0.03	4.4e-5	50772	115 / 15
10.5.2006	0.5 / 0.08	7e-5	7143	764 / 161

Supporting references and notes

S1. H. Tammet, *Atmos. Res.* **82,** 523–535 (2006).

S2. A. Hirsikko, T. Bergman, L. Laakso, M. Dal Maso, I. Riipinen., U. Hõrrak *et al., Atmos. Chem. Phys.*. **7**, 201–210, (2007).

S3. A. Mirme, E. Tamm, G. Mordas, M. Vana, J. Uin, S. Mirme *et al., Bor. Env. Res.* **12**, 247–264 (2007).

S4. N. A. Fuchs, A. G. Sutugin, *Highly Dispersed Aerosols* (London, Ann Arbor Science Publishers, 1970).

S5. P. P. Aalto, K. Hämeri, E. Becker, R. Weber, J. Salm, J.M. Mäkelä *et al*., *Tellus* **53B**, 344–358 (2001).

S6. L. Laakso, S. Gagne, T. Petaja, A. Hirsikko, P.P. Aalto, M. Kulmala *et al*., *Atmos. Chem. Phys.* **7,** 1333–1345 (2007).

S7. A. Podolsky, in *acta et commentationes Universitatis Tartuensis* 1977, 1977, no. 443, pp. 62–73.

S8. H. Tammet, in *acta et commentationes Universitatis Tartuensis* 1992, 1992, no. 947, pp. 94–115.

S9. G. Mordas, M. Kulmala, T. Petäjä, P.P. Aalto, V. Matulevicius, V. Grigoraitis *et al., Boreal Env. Res.* **10,** 543–552 (2005).

S10. M. R. Stolzenburg, University of Minnesota: Ph. D. Thesis (1988).

S11. A. Hernandez-Sierra, F.U. Alguacil, M. Alonso *J. Aerosol Sci*. **34**, 733–745 (2003).

S12. M. Heim, G. Kasper, , G. Reischl, C. Gerhard, *Aerosol Sci. Technol*, **38(S2)**, 3–14 (2004).

S13. H. Tammet, M. Kulmala, *J. Aerosol Sci.* **36**, 173–196 (2005).

S14. M. Kulmala, Hämeri, K., Aalto, P.P., Mäkelä, J.M., Pirjola, L., Nilsson, E.D. *et al.,*, *Tellus* **53B**, 324–343 (2001).

S15. A. Alam, J.-P. Shi, R. M. Harrison, *J. Geophys. Res.* **108**, 4093–4107 (2003).

S16. M. Kulmala, Dal Maso, M., Mäkelä, J.M., Pirjola, L., Väkevä, M., Aalto, P.P. *et al., Tellus* **53B**, 479–490 (2001).

S17. L. Laakso, Anttila, T., Lehtinen, K.E.J., Aalto, P.P., Kulmala, M., Hõrrak, U., *et al., Atmos. Chem. Phys.* **4**, 2353–2366 (2004).

S18. V.-M. Kerminen, M. Kulmala, *J. Aerosol Sci.*, **33**, 609–622 (2002).